



New clinical opportunities of low-field MRI: heart, lung, body, and musculoskeletal

Ye Tian¹ · Krishna S. Nayak¹

Received: 26 May 2023 / Revised: 28 September 2023 / Accepted: 5 October 2023 / Published online: 30 October 2023
© The Author(s) 2023

Abstract

Contemporary whole-body low-field MRI scanners (< 1 T) present new and exciting opportunities for improved body imaging. The fundamental reason is that the reduced off-resonance and reduced SAR provide substantially increased flexibility in the design of MRI pulse sequences. Promising body applications include lung parenchyma imaging, imaging adjacent to metallic implants, cardiac imaging, and dynamic imaging in general. The lower cost of such systems may make MRI favorable for screening high-risk populations and population health research, and the more open configurations allowed may prove favorable for obese subjects and for pregnant women. This article summarizes promising body applications for contemporary whole-body low-field MRI systems, with a focus on new platforms developed within the past 5 years. This is an active area of research, and one can expect many improvements as MRI physicists fully explore the landscape of pulse sequences that are feasible, and as clinicians apply these to patient populations.

Keywords Low-field MRI · Body MRI · Lung · Cardiac · Abdominal · Musculoskeletal · Body composition

Introduction

Clinical MRI hardware has trended towards better gradient performance (amplitude and slew rate), more sophisticated pulse sequences and reconstruction, and higher B₀ field strengths (3 T, 7 T, and beyond). The first two developments have enhanced almost all MRI applications. The trend towards higher B₀ field strength has primarily benefited high-resolution static imaging of the brain, spine, and musculoskeletal system (in the absence of metallic hardware), which are the dominant use cases for MRI in radiology today, accounting for > 70% of clinical volume. The use of higher field strengths poses several challenges for body imaging, which is the topic of this review article. Major challenges include main field (B₀) inhomogeneity, RF transmit (B₁₊) inhomogeneity, and high specific absorption rate (SAR) [1]. These limit the ability to image near tissue-air

boundaries [2], image tissue adjacent to metallic implants [3, 4], optimize image contrast, and image deep organs [5].

There has been substantial recent interest in low-field MRI systems that are paired with high-performance shielded gradients and modern consoles, specifically for body and interventional imaging. Manufacturing low-field MRI systems with modern techniques can have several advantages, such as improved B₀ homogeneity, favorable changes in NMR relaxation parameters (shorter T₁, longer T₂ and T₂*), relaxed SAR constraints, reduced acoustic noise, reduced safety concerns, and reduced manufacturing cost and total cost of ownership [6–10]. A landmark paper in 2019 by Campbell-Washburn et al. [11] introduced the opportunities for improved imaging with contemporary low-field whole-body MRI. The work was based on a commercial 1.5 T “ramped down” to 0.55 T. A few years later, Siemens announced a commercial 0.55 T scanner Free.Max [12]. Guenther et al. described opportunities availed at 0.75 T, based on a “ramped down” Philips 3 T scanner [13]. MR-Linac 0.35 T scanners [14] designed for MR-guided radiotherapy have also been leveraged to explore opportunities for general-purpose body imaging.

Diagnostic body imaging is a broad area that includes applications to the heart, lung, abdominal organs, and joints. This term notably excludes the brain and excludes

✉ Ye Tian
ytian607@usc.edu

¹ Ming Hsieh Department of Electrical and Computer Engineering, Viterbi School of Engineering, University of Southern California, 3740 McClintock Ave, EEB 406, Los Angeles, CA 90089-2564, USA

interventional applications. Imaging the trunk area has several unique challenges as artifacts can arise [15] because of cardiac and respiratory motion, susceptibility gradient between lung and tissue that results in an inhomogeneous B0 field, and the proximity of fat and lean tissues that requires fat suppression or fat/water separation. Implanted metallic hardware, such as orthopedic implants, sternal wires, and cardiac devices introduce even more significant off-resonance effects [16]. Dynamic imaging of the cardiopulmonary systems or musculoskeletal (MSK) systems may be constrained by SAR limitations [17, 18], and off resonance and short T2/T2* may limit the use of efficient long readouts [19]. These issues are all mitigated at a lower field strength, providing opportunities for improved body imaging [11].

This article reviews the application of contemporary whole-body low-field MRI systems to body imaging. Table 1 contains a high-level summary of the advantages, consequences, and newly enabled applications of this configuration. We focus on recent developments, mostly within the past five years, and do not discuss historical work that is

covered elsewhere in this special issue [20]. We do not cover interventional applications, as they are described by several other recent review papers [11, 21, 22]. We do not cover point-of-care body MRI systems [23], such as the prostate [24], or liver [25, 26] scanners, because these systems operate at a much lower field strength (<0.1 T) and are designed for a single or a few applications, and are, therefore, not suitable for general-purpose body imaging. The results discussed in this paper come primarily from whole-body systems such as the 0.35 T (Viewray) [14], 0.55 T (“ramped down” Siemens Aera [11] and Siemens Free.Max [12]), and 0.75 T (“ramped down” Philips Achieva) [13], with specifications listed in Table 2.

Cardiac imaging

Cardiac MRI is one of the major applications that benefit from high-performance low-field systems [11, 27–30]. Advantages include an improved safety profile due to lower

Table 1 Advantages of low-field MRI systems

Properties of low-field systems	Imaging consequence	Applications impacted and example references
Reduced off-resonance (includes chemical shift and susceptibility): proportional to B0	Reduced bSSFP banding artifacts	bSSFP cardiac [33, 35, 41]
	Reduced artifacts for long readouts (e.g., spiral and EPI)	Imaging near metal (e.g., orthopedic implants) [86, 89, 90]
	Reduced artifacts from metallic implants and instruments	Imaging near air spaces (lung, bowel, airway) [57–59, 63–66, 69, 92]
Reduced SAR: proportional to B0 ²	Smaller chemical shift	Water/fat separation [106]
	Allowing higher flip angles (imaging and refocusing)	bSSFP imaging where a high flip angle is contrast optimal [33]
Favorable relaxation properties: shorter T1 and longer T2/T2*	Allowing higher bandwidth pulses (higher peak B1+)	Simultaneous multi-slice imaging [40, 50]
	Stronger signal for certain sequences (e.g., bSSFP and GRE), partially compensates for the reduced SNR due to polarization	Lung parenchyma imaging [55] Improving SNR for fast gradient echo pulse sequences [41]
Enabling larger bore size	Improved patient comfort	All existing imaging [7, 92]
	Ability to image obese subjects	
	Ability to achieve different in-bore postures (e.g. side laying)	
Reduced acoustic noise	Space to perform movements during imaging	
Reduced cost (total cost of ownership)	Improved patient comfort	All existing imaging [7, 9]
	Improved access	All existing imaging [8]

Table 2 Contemporary whole-body low field (< 1 T) systems

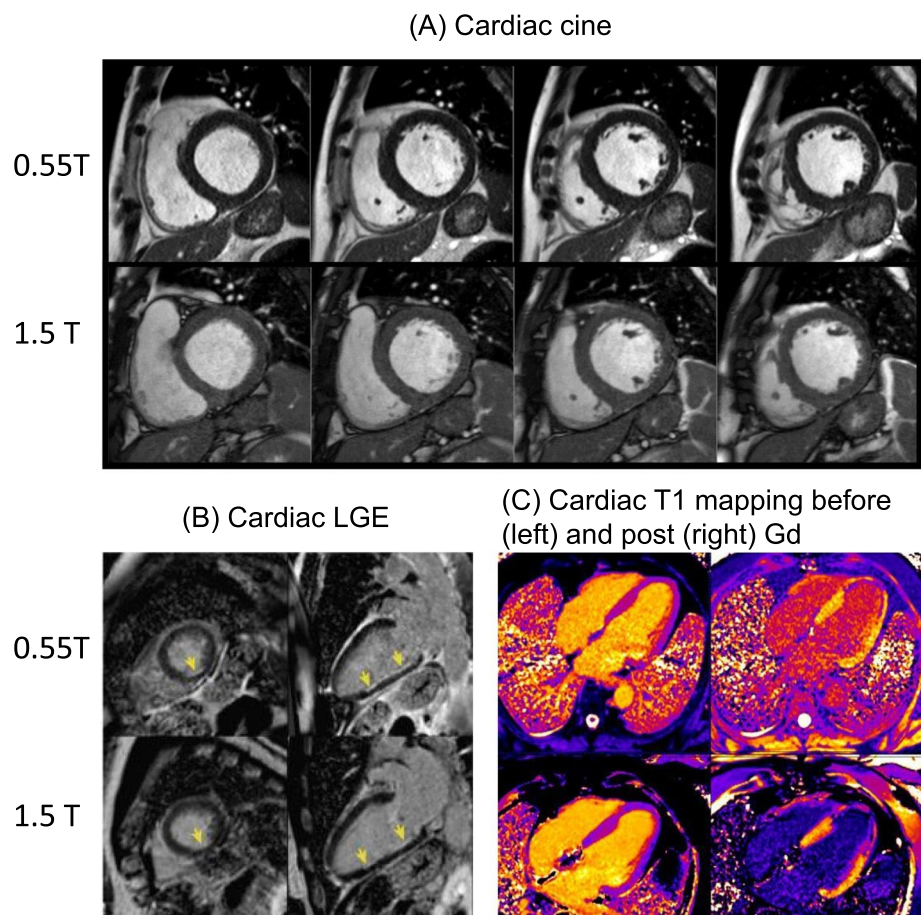
	MR-Linac	“ramped down” Aera 1.5 T	Free.Max	“ramped down” Achieva 3 T
Vendor	Viewray	Siemens	Siemens	Philips
Field strength	0.35 T	0.55 T	0.55 T	0.75 T
Maximum slew rate	200 T/m/s	200 T/m/s	40 T/m/s	200 T/m/s or 100 T/m/s
Maximum gradient amplitude	18 mT/m	45 mT/m	25 mT/m	40 mT/m or 80 mT/m
Bore size	70 cm	70 cm	80 cm	60 cm

SAR and improved device compatibility [31], improved ECG gating due to the reduced magnetohydrodynamic effect [32], and reduced off-resonance-related artifacts particularly for sequences like balanced steady-state free precession (bSSFP) [11].

An important first question to ask is whether low-field systems can achieve equivalent diagnostic performance compared to traditional field strengths, with particular attention to the reduced SNR due to polarization. Researchers have compared low-field cardiovascular magnetic resonance (CMR) with 1.5 T CMR for diagnostic performance. Rashid et al. [33] compared cine CMR at 0.35 T with 1.5 T, and found that 1.5 T cine provided higher SNR and blood-myocardium CNR, however, expert qualitative scores for high flip angle ($\geq 90^\circ$) 0.35 T cine was comparable to 1.5 T cine. Varghese et al. [34] compared cardiac function, blood flow, and myocardial tissue relaxation times between 0.35 T and 1.5 T. The study reported lower SNR at 0.35 T, but ventricular volumes, ejection fraction, peak velocity, and stroke volumes were all comparable between 0.35 T and 1.5 T or 3 T. At 0.55 T, a major effort led by intramural researchers at the National Institutes of Health (NIH) compared different cardiac sequences between 0.55 T and 1.5 T, and these included cardiac cine for functional analysis [35],

late gadolinium enhancement [36], and T1 mapping [37]. Bandettini et al. [35] compared cardiac cine between 0.55 T and 1.5 T, and found that ventricular volumes, ejection fraction, left ventricular mass, and diagnostic performance for the detection of regional wall motion abnormality were comparable. Their study focused on myocardial infarction quantification by late gadolinium enhancement imaging [38] found that both myocardial infarction mass and percentage of infarction were comparable between 0.55 T and 1.5 T. Mancini et al. [37] compared cardiac T1 mapping between 0.55 T and 1.5 T found that while T1 values are significantly lower at 0.55 T, as expected, extracellular volume fraction estimated from pre/post gadolinium T1 maps at the two field strengths showed strong agreement. Figure 1 shows representative comparisons between prototype Aera 0.55 T and 1.5 T MRI for (A) cardiac cine, (B) cardiac late gadolinium enhancement (LGE), and (C) T1 mapping. Varghese et al. have evaluated a comprehensive cardiac MRI protocol on the commercial Free.Max 0.55 T system [39], demonstrating reasonable image quality for cardiovascular structure, function, flow, and LGE assessments. Although the aforementioned studies are relatively small scale (<500 subjects), they have demonstrated diagnostic cardiac imaging at 0.35 T and 0.55 T.

Fig. 1 Comparison of cardiac MRI between 0.55 T and 1.5 T. **A** cardiac cine, reproduced from Bandettini et al. [35] **B** cardiac LGE, reproduced from Bandettini et al. [38] **C** cardiac T1 mapping, reproduced from [37]. All illustrated cardiac applications on 0.55 T show comparable diagnostic values as 1.5 T



Researchers have also studied protocol improvements to compensate for the reduced SNR due to polarization at 0.35 T [33] and 0.55 T [40], which suggest the use of higher flip angles and longer readouts. Figure 2 shows an example of bSSFP cardiac cine images acquired with different flip angles at 0.35 T and 0.55 T, demonstrating a high flip angle (usually $\geq 90^\circ$) yields the optimal blood-myocardium contrast. The use of a high flip angle at 1.5 T or 3 T is usually problematic due to the SAR constraints. Low-field systems also support contrast-optimal flip angle for simultaneous multi-slice (SMS) bSSFP, as reported by Tian et al. [40]. Restivo et al. [41] demonstrated that with an SNR efficient sampling trajectories such as spiral in–out readout, there is a 79% increase in the SNR when compared with Cartesian readout, and the SNR reduction when compared with 1.5 T Cartesian is 48% in the blood and 31% in the myocardium. These SNR-efficient techniques such as SMS and long readout may be problematic at higher field strength due to increased SAR and off-resonance artifacts. On the 0.75 T system, Peereboom et al. [42] measured T1, T2, and T2* in the myocardium, and demonstrated that by leveraging these physical prosperities in the pulse sequence design accurate myocardial spectroscopy measurement can be achieved at 0.75 T.

Real-time cardiac imaging is promising at low field since the ability to use long readouts (such as spiral or echo-planar [41]) dramatically improves scan efficiency. Real-time imaging generally provides simplified and patient-friendly scanning because it does not rely on breath-holds or ECG gating. However, the use of non-Cartesian trajectories and

high undersampling factors can limit the speed of online reconstruction. In cases where low-latency is needed, through-time GRAPPA [43, 44] and machine learning-based reconstructions [45] have been shown to provide reconstruction with ≤ 200 ms latency [46]. At low field, Fyrdahl et al. [47] demonstrated the feasibility of through-time GRAPPA for real-time cardiac MRI on the Free.Max 0.55 T. On the same system, Hamilton et al. [48] developed a deep-learning reconstruction for real-time cardiac MRI. Real-time cardiac MRI capability is greatly improved by leveraging the ability to use longer readouts, flexibility of trajectory design, and relaxed SAR constraints. These have been demonstrated on the prototype Aera 0.55 T system. Wang et al. [49] developed a spiral in–out sequence for real-time cardiac cine, which provides improved scan efficiency and achieves TE approximately equal to TR/2. Yagiz et al. [50] developed an SMS bSSFP technique at 0.55 T to achieve real-time simultaneous multiple-slice coverage, enabling more comprehensive real-time cardiac function assessment.

To date, several pilot studies have demonstrated the feasibility of low-field CMR for cardiac function, tissue characterization, flow measurements, and LGE imaging. Some functional assessments may be worse at low field, such as those based on feature tracking [51] and tagging [52], due to the need for high SNR and/or long myocardial T1 for tag persistence. Myocardial first-pass perfusion can benefit from expanded coverage and a finer spatial resolution, that low-field systems may be able to provide [53]. CMR at low field may also provide reduced safety concerns and reduced imaging artifacts for patients with cardiac implanted devices [54],

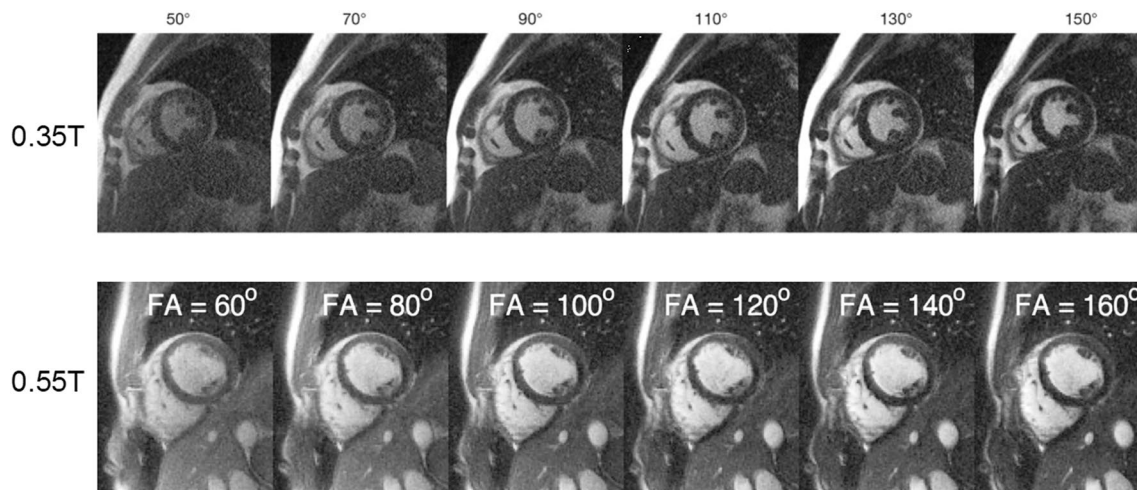


Fig. 2 Blood-myocardium contrast changes with a flip angle. The apparent contrast between the blood and the myocardium increases as the bSSFP flip angle increases and peaks at flip angle = 130° at 0.35 T and at flip angle = 160° at 0.55 T. Note that the blood signal is not in a steady state due to the constant inflow in the ventricular, which increases the signal intensity. This resulted in a higher contrast-optimal flip angle in the experiment than in the steady-state Bloch simu-

lation. A high flip angle can be applied within a reasonable TR without exceeding the SAR limitation on low-field systems. At 1.5 T or 3 T, applying a high flip angle may prolong the TR, which can introduce more banding artifacts for bSSFP cine. 0.35 T images are reproduced from Rashid et al. [33] and the 0.55 T images are reproduced from Tian et al. [40]

providing improved access and screening for such patients. Clinical evaluation of real-time CMR is still needed to assess its robustness and workflow improvements. The focus should be on patients with arrhythmia or those who experience difficulties in maintaining breath-holding during the imaging process.

Lung imaging

Lung imaging is an application that is currently dominated by computed tomography (CT), where low-field MRI could provide a breakthrough [11]. CT provides excellent spatial resolution in a short scan time, but requires exposure to ionizing radiation, and has difficulty characterizing tissues (e.g., differentiating benign from malignant lung nodules). The radiation dose is a constraint when deciding the frequency of monitoring, use in children, and feasibility of dynamic assessments. MRI, being a radiation-free modality that is excellent for tissue characterization, has the potential to alleviate these constraints. Lung MRI at conventional field strengths is limited by the extremely short $T2^*$ in parenchyma (due to the numerous air-tissue interfaces from alveoli). This is a much relaxed constraint at low field and can greatly improve structural imaging and functional assessments of the lung.

At low field, lung parenchyma $T2/T2^*$ values are greatly prolonged, providing high SNR efficiency. Li et al. [55] jointly measured the lung parenchyma $T2/T2^*$ with an echo-shifted multi-echo spin echo pulse sequence, determining the normative values of lung parenchyma are $T2 = 68.6$ ms and $T2^* = 8.2$ ms. Notably, the $T2^*$ is 5–10 times larger than at 1.5 T (2.11 ms) or 3 T (0.74 ms) [56]. This greatly improves the capability of performing lung imaging at low field strengths, and many opportunities are emerging. Campbell-Washburn et al. [57] demonstrated diagnostic image quality with a T2-weighted spin echo sequence in a small cohort of

patients ($N = 24$) with various lung conditions, with representative examples shown in Fig. 3. T2-weighted sequences at 0.55 T provide important structural assessments of many lung conditions. Combined with a diffusion weighted imaging, differentiation of benign and malignant lung nodules was also possible [58]. T2-weighted structural images were also used to assess pulmonary ground glass and fibrosis-like opacities associated with COVID-19 [59–61]. Hinsen et al. [62] compared lung nodule detection between 0.55 T MRI and CT. In 964 total nodules of 46 patients, MRI had 100% accuracy in detecting nodules of size ≥ 6 mm, 80% (159/200) for those ≥ 4 and < 6 mm, and 23% (147/638) for those < 4 mm.

Ultra-short TE (UTE) imaging, by using extremely short excitation pulses and center-out readouts, can overcome the short $T2^*$ limitation at high field strengths. UTE has been used with great success, however, is limited by short readout time (< 2 ms) and poor scan efficiency. At low field, UTE pulse sequences can be combined with long spiral readout to achieve improved scan efficiency. Bhattacharya et al. [63] studied the use of breath-held spiral UTE to evaluate regional lung ventilation based on the T1-shortening effect of inhaled 100% O_2 (compared to room air). By using a 7-ms spiral readout, the sequence achieved $3.5 \times 3.5 \times 10$ mm³ whole-lung coverage in a short 9-s breath-hold. This combined with a T2-weighted BLADE pulse sequence enabled joint assessment of lung function and structure in patients with lymphangioliomyomatosis (LAM) [64]. Javed et al. [65] have demonstrated a free-breathing UTE spiral pulse sequence for 3D lung imaging, achieving 1.75 mm isotropic resolution whole-lung imaging in 8 min. This pulse sequence was further used to study the lung water density, where it was shown that with a lower spatial resolution at 3.5 mm isotropic and 1° flip angle it was sensitive enough to capture lung water redistribution under gravity [66]. bSSFP with an extremely short TR (~ 2 ms) can provide high-quality lung structure imaging at 1.5 T [67, 68]. This approach has

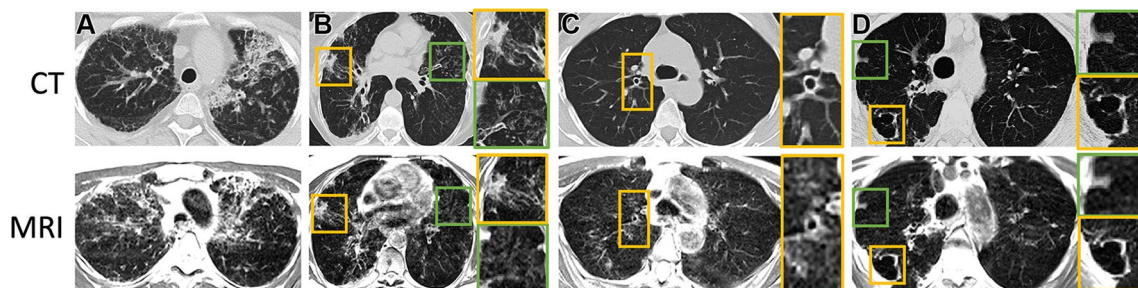


Fig. 3 Axial CT (reformatted to $0.8 \times 0.8 \times 6$ mm) and T2-weighted MR (reformatted to $1.1 \times 1.1 \times 6$ mm) images show **A** honeycombing, interstitial thickening, and fibrotic changes in a 35-year-old woman; **B** consolidative opacities in a 70-year-old woman; **C** bronchial wall thickening with bronchiectasis in a 58-year-old woman; and **D** a cavi-

tary lesion in a 70-year-old woman. **B–D** Green and yellow boxes on CT and MR images denote the area of interest around the particular finding described, with the corresponding box bordered in that color to the right of the respective image showing an enlarged view of the area. Image is reproduced from Campbell-Washburn et al. [57]

recently been shown to achieve sub-millimeter lung imaging at 0.55 T [69].

Hyperpolarized ^3He imaging is also promising at the low field since the polarization is not dependent on field strength, the increased T2 and T2*, and reduced susceptibility gradients enabled more flexible and efficient readouts. Though there are no studies investigating hyperpolarized lung imaging with contemporary low-field systems, some other works are worth mentioning. Komlosi et al. [70] studied the SNR, T2, and T2* with hyperpolarized ^3He at different field strengths (0.43 T, 0.79 T, and 1.5 T), finding the SNR weakly depended on field strength, however, there is a large increment in T2 and T2* values at lower field strengths, as expected. An earlier work by Salerno et al. [71] reported a threefold increment in hyperpolarized ^3He T2* value at 0.54 T compared with 1.5 T, and reduced spiral blurring induced by susceptibility effects.

Abdominal imaging

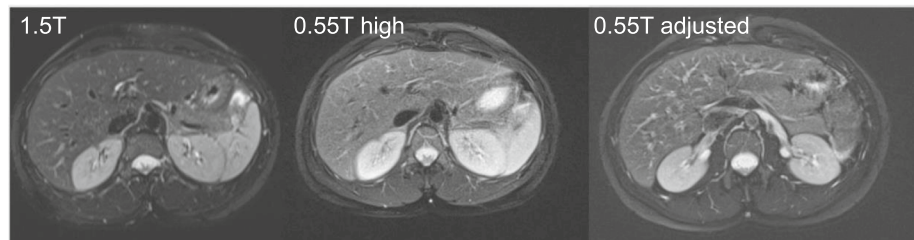
Abdominal imaging is challenging because of the large field-of-view (FOV) requirement, inhomogeneous B0 field due in part to gas in the gastrointestinal (GI) tract, and complex motion from breathing and gastrointestinal movements. Abdominal imaging can benefit from low-field systems,

due to the improved B0 field homogeneity, reduced artifact near lung air or GI gas, and reduced artifacts near metallic implants [72]. Low-field systems may also be made with larger bore size, enabling imaging for obese patients [73]. Relaxed constraints in pulse sequence design such as enabling large FOV bSSFP, reduced SAR, and enabling longer readout also benefit dynamic imaging, for example, studies for GI movements or motion-resolved abdominal imaging [74].

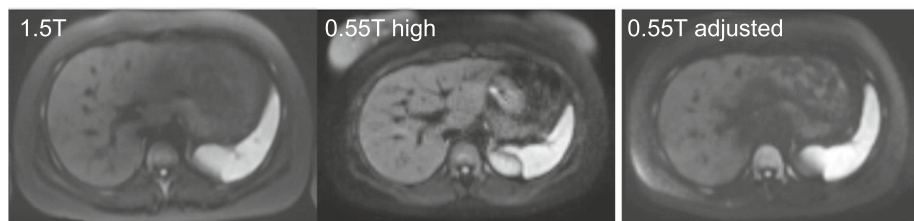
Despite the promises of low-field abdominal imaging, there is little published work in this area. Chandarana et al. [75] developed a protocol for abdominal imaging at 0.55 T. In 10 healthy volunteers, the group demonstrated diagnostic quality images with fat-saturated T2 weighting, diffusion weighting, and Dixon T1 weighting in a total acquisition time of 10 min. Representative images from this protocol are shown in Fig. 4. Ramachandran et al. [76] compared 0.55 T MRI and 1.5 T MRI of the abdomen in 15 healthy volunteers, finding that the 0.55 T achieved an acceptable image with a prolonged scan time. Issues that warrant further investigation are low SNR, insufficient fat suppression, and aliasing due to undersampling. Liu et al. [77] have studied the use of Rosette MR fingerprinting for quantifying T1, T2, and water-fat separation in the liver at 0.55 T. The use of Rosette trajectory provides multiple echoes for water-fat separation, and the noise-resilient fingerprinting

Fig. 4 Representative liver images at 1.5 T, 0.55 T with a high gradient, and 0.55 T with an adjusted gradient. **A** T2 weighted images **B** high b-value diffusion-weighted images **C** T1 weighted fast spin echo images. Each row shows images acquired at 1.5 T (left), 0.55 T with “ramped down” Aera gradient performance (middle), and 0.55 T with gradient performance adjusted to the same as Free.Max

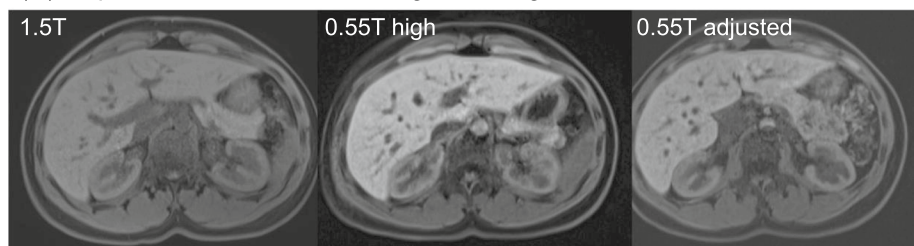
(A) Representative T2 weighted images



(B) Representative high b-value diffusion weighted images



(C) Representative fat-sat T1 weighted images



with longer readouts can partially overcome the low SNR issue at low field. Another fingerprinting work performed at 0.75 T also targeted at water/fat-separated parameter mapping in the abdomen but with a spiral multi-echo acquisition [78]. Future studies are needed to investigate the diagnostic performance of low-field MRI for specific diseases and to develop methods to suppress confounding artifacts. Opportunities exist in exploring applications that benefit from reduced off-resonance artifacts around gas and in a larger FOV.

Musculoskeletal imaging

Contemporary low-field systems may provide diagnostic images for most MSK applications. Khodarahmi et al. [79] reviewed MSK applications at low field and posed challenges and opportunities in this area. The low SNR at low field is the largest challenge for general MSK applications since MSK applications generally require fine spatial resolution and high contrast to identify injuries or degenerative disorders. Solutions to these issues include the use of longer scan time and AI-based denoising. Another major challenge in MSK at the low field is water-fat separation. As the water fat chemical shift frequency is smaller at lower field strength, water or fat suppression preparation pulses are prolonged and are not as effective [80]. Short tau inversion recovery (STIR) can be applied to effectively suppress the fat signal at low field, albeit with reduced flexibility in image contrast [81]. Despite the challenges, low-field systems may have several advantages over higher-field strength systems in imaging near metallic implants and dynamic imaging of the MSK system. These advantages mainly come from the reduced susceptibility effects and improved dynamic imaging capability.

A few early and recent cross-field strength comparison studies have demonstrated the diagnostic capability of several MSK applications at low field. In an early study done in 1996, Rutt et al. [82] demonstrated no diagnostic difference between early 0.5 T and 1.5 T scanners for anterior cruciate ligament tears in the knee. A recent study compared lumbar spine images in healthy volunteers acquired at both 0.55 T and 1.5 T [83]. The study revealed that the image quality at 0.55 T is perceived to be lower than 1.5 T. The 0.55 T images underwent denoising using a machine learning tool provided by the vendor (Deep Resolve Gain/Sharp, Siemens Healthcare, Erlangen, Germany), resulting in improved image quality. Although the denoised 0.55 T images were still rated lower than 1.5 T images, they were in the good to perfect range and were acquired with a reduced scan time. With the same deep learning tool, Schmidt et al. [84] demonstrated that deep learning enhanced MRI images at 0.55 T

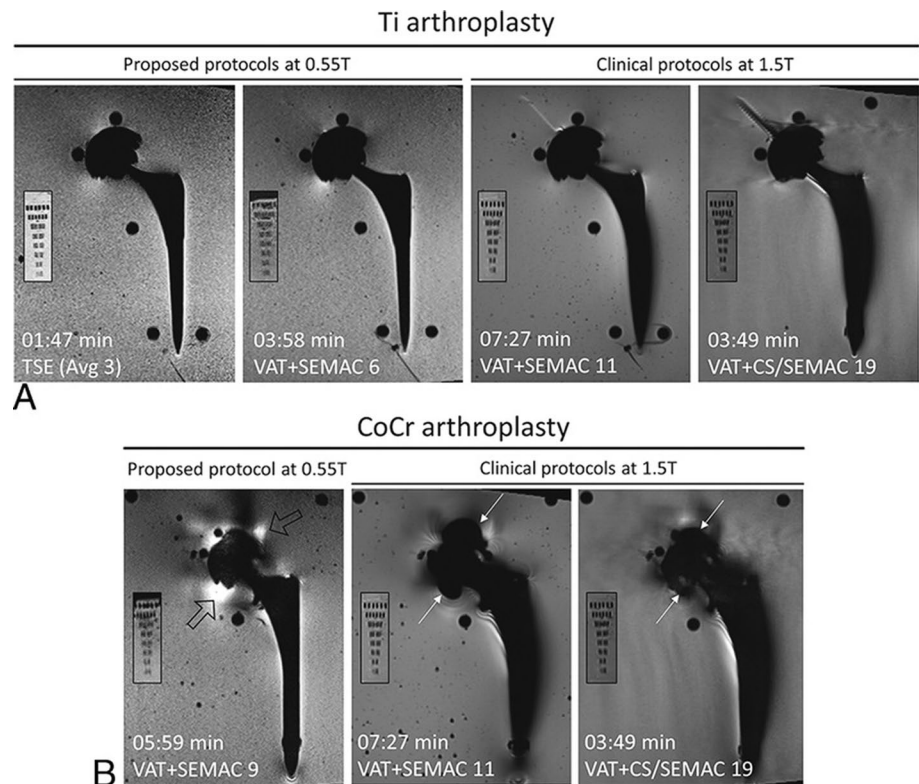
could achieve equivalent diagnostic accuracy compared to 1.5 T MRI for knee structural and pathological diagnosis.

Low-field systems have the potential to significantly enhance the ability of imaging around metallic implants. Depending on the material, size, shape, and orientation, metallic implants create different levels of imaging artifacts at different field strengths [16, 85], due to the large susceptibility gradients generated by metal. Certain materials have consistent artifacts across field strengths [86, 87]; however, most materials produce artifacts that scale with field strength. Consequently, imaging tissues adjacent to metallic implants becomes more challenging at higher field strengths [88]. At lower field strengths, susceptibility effects are much smaller, such that the distortion, signal void, and signal pile-up effects are much reduced. Khodaremi et al. [89] have compared hip implant phantom imaging using SEMAC between 0.55 and 1.5 T and found that with an optimized protocol the 0.55 T MRI has a 45–64% smaller artifact size compared with 1.5 T MRI, with only a minor SNR penalty at 17–28%. Representative hip implant phantom images acquired at 0.55 T and 1.5 T are shown in Fig. 5. Keskin et al. [90] studied the use of gradient sequences to obtain high-resolution images near metallic implants, which is usually not feasible at higher field strengths.

Dynamic imaging of the MSK systems is also promising in contemporary low-field systems. These systems allow for longer readouts, higher flip angle, and bSSFP imaging. Lim et al. [91] studied the use of real-time bSSFP sequence for speech imaging at 0.55 T, reporting superior image quality than spoiled gradient echo (GRE) sequence at the same and higher field strengths. The feasibility of using real-time MRI for assessing wrist movement instability with a high spatial resolution was also demonstrated at the ramped-down Aera 0.55 T system [92].

Several low-field open-bore systems also have a role in clinical MSK imaging, such as the G-scan Brio 0.25 T (Esaote) and the MrOpen 0.5 T (Paramed). These systems are specially designed to support imaging at multiple body positions, including but not limited to supine, sitting, and standing, each poses a different weight loading (e.g., in the knee or the spine). Comparison of MSK under different realistic weight loading conditions can better elucidate pathology and the underlying reason for symptoms including pain. Alessandra et al. [93] reported the use of a 0.25 T system for assessing lumbar spine instability over 10 years on 4305 patients. When imaging at both supine and standing positions, they were able to assess disc diseases that were undetected when imaging in the supine position alone. Morphological changes in the spine under different loading conditions were also reported by Nordberg et al. [94] with the same scanner. At 0.5 T, Aarvold et al. [95] reported femoral head deformity under weight bearing in children with Legg-Calve-Perthes disease. Pai et al. [96] studied

Fig. 5 Comparison of 0.55 T optimized pulse protocols with clinical 1.5 T View Angle Tilting (VAT)+ Slice Encoding for Metal Artifact Correction (SEMAC) and VAT+CS/SEMAC pulse sequences for Ti (A) and CoCr (B) implants. Smaller panels show the resolution phantom in each case. Metal artifacts are significantly reduced primarily surrounding the femoral stem for both implant types. Areas of signal loss around the CoCr acetabular cup at 1.5 T (white arrows) are replaced by smaller areas of signal pileup at 0.55 T (hollow arrows). Image is reproduced from Khodarahmi et al. [89]



muscle morphology changes in the thorax with the level and posture of healthy volunteers. Charest-Morin et al. [97] studied dynamic morphometric changes in the spine between supine and standing positions in patients with degenerative spondylolisthesis.

Small bore low-field “extremity” MRI systems can be made with more compact sizes since only one limb needs to fit, and a dedicated scanner shape and coil for the targeted region of interest can be designed [98, 99]. A few studies have evaluated the diagnostic performance of the E-scan 0.2 T shoulder system, generally supporting its usefulness in the diagnosis of conditions such as rotator cuff and labral lesions [100, 101]. Wrist and finger joints assessments using the 0.2 T Artsocan system were also studied [102–104], supporting the cost-effectiveness and accuracy of the diagnosis.

Body composition

Whole body composition or organ-specific body composition measurements are valuable biomarkers of obesity, metabolic disease, muscle disorders, and diagnostic references. This usually requires water/fat-separated imaging to quantify the fat–water proton density ratio. Low-field systems may provide improved body composition measurements by enabling larger bore size, reducing acoustic noise, and reducing scan time by leveraging time-efficient readouts. At low field strength, there are unique technique challenges for water/fat

separation or spectrum excitation. ^1H in water and fat experience different chemical shifts. The difference between water (single-peak) and the dominant peak in lipids is approximately 3.5 parts per million. The difference in off-resonance frequencies (Δf) is directly proportional to the field strength. The smaller Δf at low field makes it less practical to apply frequency selective pulses, since these pulses would require longer duration (roughly 1–2 times the reciprocal of Δf , e.g., 12–24 ms at 0.5 T). Methods that separate water and fat components, such as the multiple echo Dixon method [105], can be used to achieve water or fat suppression effectively. Nayak et al. [106] recently optimized a 2-point Dixon protocol for body composition profiling at 0.55 T. Several works have targeted more sophisticated optimization of Dixon methods at low field, including a 3-point Dixon at 0.75 T [107], and a combination with non-Cartesian trajectories to achieve improved scan efficiency [108] or motion robustness [109]. Tian et al. have demonstrated a bSSFP spiral out-in-out-in sequence for real-time water/fat separation [110]. The use of bSSFP pulse sequence and spiral readout improves the SNR efficiency, allowing real-time imaging with sufficient SNR for water/fat separation. However, the drawback of bSSFP is its susceptibility to banding artifacts and signal void, which can pose challenges for fat fraction quantification.

Zi et al. [111] demonstrated a frequency offset method applied to adiabatic spectrally selective inversion pulse for effective fat suppression in abdominal imaging. Instead

of designing an effective fat suppression pulse, the work exploits a short preparation pulse but sweeps a range of RF frequencies and uses the frequency response to perform effective water and fat separation. Note that the scan time is prolonged due to the frequency sweeping, however, the redundancy of data may allow for more sparse sampling with constrained reconstruction.

Technical challenges and opportunities

There are known issues at low field, namely the concomitant field effects and the lower SNR due to polarization. Lee et al. [112] have addressed the concomitant field problems for GRE-based spiral sequences in the MaxGIRF framework. MaxGIRF uses a model-based reconstruction and can simultaneously correct the off-resonance and concomitant fields blurring, but a separate measurement of the off-resonance map is needed. The group is also extending the work to include gradient nonlinearities in the reconstruction modeling [113]. Wang et al. [114] have developed a modification to the spiral-ring spin echo pulse sequences to compensate for concomitant field effects. This method nulls the concomitant field at the echo time by modifying the gradient, and when combined with reconstruction-based concomitant field correction and off-resonance correction, imaging blurring in spiral imaging is substantially reduced. With a similar approach, Ramasawmy et al. [115] compensated concomitant field for a turbo spin echo spiral in–out sequence.

Pilot tone [116] is a promising technique to capture respiratory and cardiac physiological signals without the need of external device or image navigator, by incorporating the motion signal into the acquired data, just outside of the imaging bandwidth. Pilot tone is applicable at all field strengths, and there are relatively minor (but non-trivial) technical challenges to getting consistent performance across field strengths due to the different operating frequencies [117]. Solomon et al. [118] demonstrated the feasibility of pilot tone on an Aera 0.55 T scanner, capturing a good quality respiratory signal that could be used to guide image reconstruction. Obtaining a reliable cardiac signal using pilot tone at low field remains an open challenge. As modern low field scanners are emerging recently, some of the product models have built-in pilot tone support such as Siemens Free.Max. Pilot tone may generally benefit free-breathing body imaging when respiratory motion needs to be resolved.

Application-specific coil design can greatly improve image SNR, parallel imaging performance, and sensitivity to the desired FOV. These have been demonstrated in the application of speech production [119] and in the knee [120] at 0.55 T. Coils designs are field-strength and frequency

dependent, and improvements can be expected as more effort is dedicated to improved low-field body coils.

Powerful new tools based on machine learning are being used to enhance MRI capabilities [121, 122]. Example uses include image reconstruction and denoising [123–125], trajectory optimization [126–128], automated scan planning [129, 130], and automated analysis [131–133]. Although studies focusing on low-field strength (especially 0.1–1 T) are still rare, low-field MRI is expected to greatly benefit from these advances. Low-field MRI generally suffers from lower SNR due to lower equilibrium polarization, therefore we expect that denoising algorithms using machine learning may effectively mitigate this issue [134–136]. Machine learning can also contribute to sampling strategy optimization. Since low-field systems allow substantially greater flexibility in the design of sampling trajectories, longer readouts, and the utilization of high B1+ pulses, machine learning is expected to be a powerful aid in searching a broad parameter space to identify optimized solutions for specific applications. Machine learning also has a significant impact on scanning and analysis through automation. This potential reduction in the need for specialized personnel training can further lower operational costs associated with low-field systems, ultimately facilitating greater access to MRI services.

Discussion

We have reviewed the body applications of contemporary low-field (< 1 T) MRI scanners. Most of the research has focused on the optimization of clinical protocols and demonstrating the feasibility or baseline diagnostic performance of these scanners, by using well-established 1.5 T MRI, 3 T MRI, or CT as a reference. To our knowledge, clinical non-inferiority studies have not been performed to date. These are expensive and difficult to perform, as they require very large numbers of subjects, and require each subject to undergo multiple exams.

Contemporary high-performance low-field MRI systems provide comparable and in many cases superior-performance body imaging compared to high-field counterparts. The reduced off-resonance and relaxed SAR provide substantially increased flexibility in the design of MRI pulse sequences. This is an active area of research, and one can expect many improvements in the coming years, as MRI physicists fully explore the broader range of pulse sequences that are feasible, and as clinicians apply these to patient populations.

Low-field outperforms conventional field strengths for some applications, notably lung imaging (because of the substantially longer T2*) and imaging immediately adjacent to metallic implants (because of the reduced susceptibility-induced off-resonance). We anticipate that

low-field MRI may become the premier platform for these and other applications. Computed Tomography (CT) is the leading modality for diagnosis and evaluation of lung diseases. This is largely due to the limited imaging options in the lung, though the added radiation dose is of concern for certain patient groups such as young children or patients who need repeated scans. Low-field MRI has the potential to replace CT in certain applications, such as lung function evaluation [63], early detection of lung nodules [62], and evaluation of cystic fibrosis. Imaging around metallic implants is another application that low-field MRI has clear advantages over higher field strengths [89]. SNR remains as an issue due to the lower equilibrium polarization, and the need for very high spatial resolution. This is an area where novel multi-spectral imaging pulse sequences and reconstructions and/or machine learning may be helpful.

It remains an open question whether low-field MRI will gain broad traction prior to large-scale studies demonstrating clinical non-inferiority (compared to standard 1.5 T or 3 T MRI). Several small-scale studies have already demonstrated the diagnosis accuracy of low-field MRI, such as for cardiac [33–35, 38, 39], MSK [79], and abdominal [75] applications. These studies have also documented differences in image quality which trend as expected with field-strength differences that would be expected based on MRI physics.

Low-field MRI may enable novel evaluation of normal and abnormal body dynamics, such as joint movement [92, 137], bowel motility [110], swallowing/aspiration [139], and airway collapse [140]. These have been attempted at conventional field strengths but were difficult to make robust for widespread use. Dynamic MRI appears to be more robust at low-field, and this may provide a new suite of applications for MRI as a whole. Quantitative imaging at low field may provide new clinical insights because of relaxometry changes (shorter T1 and longer T2/T2*), Reference tissue quantification values need to be reestablished for each different field strength or different scanner [141, 142]. Another major promise of low-field MRI is improved accessibility. The reduced cost of ownership, reduced carbon footprint, and less liquid helium requirements could extend MRI services to areas that previously had limited access. It is often necessary to increase scan time to achieve acceptable image quality [39, 76, 79], which suggests the need to evaluate cost-effectiveness for low-field MRI systems. Improved patient comfort with reduced acoustic noise, larger bore size design, and improved safety, could bring MRI serve to people that was previously underserved [6, 7, 9, 143].

Acknowledgements Y.T. and K.S.N. receive grant support from the National Institutes of Health (Nos. R21-HL159533, R01-AR078912, U01-HL167613), National Science Foundation (No. 1828736), and American Heart Association (No. 903839), and receive research support from Siemens Healthineers.

Funding Open access funding provided by SCEL, Statewide California Electronic Library Consortium.

Declarations

Conflict of interest The authors have no conflict of interest to disclose.

Ethical standards The authors receive research support from Siemens Healthineers.

Open Access This article is licensed under a Creative Commons Attribution 4.0 International License, which permits use, sharing, adaptation, distribution and reproduction in any medium or format, as long as you give appropriate credit to the original author(s) and the source, provide a link to the Creative Commons licence, and indicate if changes were made. The images or other third party material in this article are included in the article's Creative Commons licence, unless indicated otherwise in a credit line to the material. If material is not included in the article's Creative Commons licence and your intended use is not permitted by statutory regulation or exceeds the permitted use, you will need to obtain permission directly from the copyright holder. To view a copy of this licence, visit <http://creativecommons.org/licenses/by/4.0/>.

References

- Ladd ME, Bachert P, Meyerspeer M, Moser E, Nagel AM, Norris DG et al (2018) Pros and cons of ultra-high-field MRI/MRS for human application. *Prog Nucl Magn Reson Spectrosc* 109:1–50
- Farahani K, Sinha U, Sinha S, Chiu LC, Lufkin RB (1990) Effect of field strength on susceptibility artifacts in magnetic resonance imaging. *Comput Med Imaging Graph* 14(6):409–413
- Ho HS (2001) Safety of metallic implants in magnetic resonance imaging. *J Magn Reson Imaging* 14(4):472–477
- Hori M, Hagiwara A, Goto M, Wada A, Aoki S (2021) Low-field magnetic resonance imaging: its history and renaissance. *Invest Radiol* 56(11):669–679
- Graves MJ (2022) 3 T: the good, the bad and the ugly. *Br J Radiol* 95(1130):20210708
- Arnold TC, Freeman CW, Litt B, Stein JM (2023) Low-field MRI: clinical promise and challenges. *J Magn Reson Imaging* 57(1):25–44
- Rusche T, Vossenrich J, Winkel DJ, Donners R, Segeroth M, Bach M et al (2022) More space, less noise—new-generation low-field magnetic resonance imaging systems can improve patient comfort: a prospective 0.55T–1.5T-scanner comparison. *J Clin Med* 11(22):6705
- Vossenrich J, Breit HC, Bach M, Merkle EM (2022) Economic aspects of low-field magnetic resonance imaging: acquisition, installation, and maintenance costs of 0.55 T systems. *Radiologe* 62(5):400–404
- Dillinger H, Kozerke S, Guenther C (2022) Direct comparison of gradient fidelity and acoustic noise of the same MRI system at 3 T and 0.75 T. *Magn Reson Med* 88(4):1937–1947
- Gilk T, Kanal E (2023) MRI safety considerations associated with low-field MRI: mostly good news. *MAGMA* 36(3):427–428
- Campbell-Washburn AE, Ramasawmy R, Restivo MC, Bhattacharya I, Basar B, Herzka DA et al (2019) Opportunities in interventional and diagnostic imaging by using high-performance low-field-strength MRI. *Radiology* 293(2):384–393
- Healthineers S (2020) Siemens Healthineers moves into new clinical fields with its smallest and most lightweight whole-body

- MRI. <https://www.siemens-healthineers.com/press-room/press-releases/magnetom-free-max.html>
13. Guenther C, Peereboom SM, Dillinger H, McGrath C, Albanay MM, Vishnevskiy V et al (2023) Ramping down a clinical 3 T scanner: a journey into MRI and MRS at 0.75 T. *MAGMA* 36:355–373
 14. Klüter S (2019) Technical design and concept of a 0.35 T MR-Linac. *Clin Transl Radiat Oncol*. 18:98–101
 15. Krupa K, Bekiesińska-Figatowska M (2015) Artifacts in magnetic resonance imaging. *Pol J Radiol* 80:93–106
 16. Hargreaves BA, Worters PW, Pauly KB, Pauly JM, Koch KM, Gold GE (2011) Metal-induced artifacts in MRI. *AJR Am J Roentgenol* 197(3):547–555
 17. Oshinski JN, Delfino JG, Sharma P, Gharib AM, Pettigrew RI (2010) Cardiovascular magnetic resonance at 3.0 T: current state of the art. *J Cardiovasc Magn Reson* 12(1):55
 18. Shapiro L, Harish M, Hargreaves B, Staroswiecki E, Gold G (2012) Advances in musculoskeletal MRI: technical considerations. *J Magn Reson Imaging* 36(4):775–787
 19. Haskell MW, Nielsen JF, Noll DC (2023) Off-resonance artifact correction for MRI: a review. *NMR Biomed* 36(5):e4867
 20. Hennig J (2023) An evolution of low-field strength MRI. *MAGMA* 36(3):335–346
 21. Thompson SM, Gorny KR, Koepsel EMK, Welch BT, Mynderse L, Lu A et al (2021) Body interventional MRI for diagnostic and interventional radiologists: current practice and future prospects. *Radiographics* 41(6):1785–1801
 22. Rogers T, Campbell-Washburn AE, Ramasawmy R, Yildirim DK, Bruce CG, Grant LP et al (2023) Interventional cardiovascular magnetic resonance: state-of-the-art. *J Cardiovasc Magn Reson* 25(1):48
 23. Webb A, O'Reilly T (2023) Tackling SNR at low-field: a review of hardware approaches for point-of-care systems. *MAGMA* 36(3):375–393
 24. Sze C, Singh Z, Punyala A, Satya P, Sadinski M, Narayan R et al (2023) Feasibility and preliminary clinical tolerability of low-field MRI-guided prostate biopsy. *Prostate* 83(7):656–662
 25. Barahman M, Grunvald E, Prado PJ, Bussandri A, Henderson WC, Wolfson T et al (2022) Point-of-care magnetic resonance technology to measure liver fat: Phantom and first-in-human pilot study. *Magn Reson Med* 88(4):1794–1805
 26. Wang Y, Xu Y, Zhang M, Emmanuel Komolafe T, Wang W, Luo H et al (2021) A single-sided magnet for deep-depth fat quantification. *J Magn Reson* 331:107053
 27. Qin C, Murali S, Lee E, Supramaniam V, Hausenloy DJ, Obungoloch J et al (2022) Sustainable low-field cardiovascular magnetic resonance in changing healthcare systems. *Eur Heart J Cardiovasc Imaging* 23(6):e246–e260
 28. Simonetti OP, Ahmad R (2017) Low-field cardiac magnetic resonance imaging: a compelling case for cardiac magnetic resonance's future. *Circ Cardiovasc Imaging* 10(6):e005446
 29. Nayak KS, Lim Y, Campbell-Washburn AE, Steeden J (2022) Real-time magnetic resonance imaging. *J Magn Reson Imaging* 55(1):81–99
 30. Campbell-Washburn AE, Varghese J, Nayak KS, Ramasawmy R, Simonetti OP (2023) Cardiac MRI at low field strengths. *J Magn Reson Imaging*. <https://doi.org/10.1002/jmri.28890>
 31. Strach K, Naehle CP, Mühlsteffen A, Hinz M, Bernstein A, Thomas D et al (2010) Low-field magnetic resonance imaging: increased safety for pacemaker patients? *Europace* 12(7):952–960
 32. Fischer SE, Wickline SA, Lorenz CH (1999) Novel real-time R-wave detection algorithm based on the vectorcardiogram for accurate gated magnetic resonance acquisitions. *Magn Reson Med* 42(2):361–370
 33. Rashid S, Han F, Gao Y, Sung K, Cao M, Yang Y et al (2018) Cardiac balanced steady-state free precession MRI at 0.35 T: a comparison study with 1.5 T. *Quant Imaging Med Surg* 8(7):627–636
 34. Varghese J, Craft J, Crabtree CD, Liu Y, Jin N, Chow K et al (2020) Assessment of cardiac function, blood flow and myocardial tissue relaxation parameters at 0.35 T. *NMR Biomed* 33(7):e4317
 35. Bandettini WP, Shanbhag SM, Mancini C, McGuirt DR, Kellman P, Xue H et al (2020) A comparison of cine CMR imaging at 0.55 T and 1.5 T. *J Cardiovasc Magn Reson* 22(1):37
 36. Bandettini WP, Shanbhag SM, Mancini C, Henry JL, Lowery M, Chen MY et al (2021) Evaluation of myocardial infarction by cardiovascular magnetic resonance at 0.55-T compared to 1.5-T. *JACC Cardiovasc Imaging* 14(9):1866–1868
 37. Mancini C, Bandettini WP, Kellman P, Xue H, Campbell-Washburn AE (eds) (2021) Comparison of cardiac T1 mapping on a high-performance 0.55T scanner and a conventional 1.5T scanner. In: 2021 ISMRM & SMRT Annual Meeting & Exhibition; 2021; Virtual, p S31
 38. Bandettini W, Shanbhag S, Mancini C, Henry J, Lowery M, Chen M (2021) Evaluation of myocardial infarction by CMR at 0.55T compared to 1.5T. *JACC Cardiovasc Imaging* 14(9):1866–1868
 39. Varghese J, Jin N, Giese D, Chen C, Liu Y, Pan Y et al (2023) Building a comprehensive cardiovascular magnetic resonance exam on a commercial 0.55 T system: a pictorial essay on potential applications. *Front Cardiovasc Med*. 10:1120982
 40. Tian Y, Cui SX, Lim Y, Lee NG, Zhao Z, Nayak KS (2022) Contrast-optimal simultaneous multi-slice bSSFP cine cardiac imaging at 0.55 T. *Magn Reson Med* 89:746–755
 41. Restivo MC, Ramasawmy R, Bandettini WP, Herzka DA, Campbell-Washburn AE (2020) Efficient spiral in-out and EPI balanced steady-state free precession cine imaging using a high-performance 0.55T MRI. *Magn Reson Med* 84(5):2364–2375
 42. Peereboom SM, Guenther C, Albanay MM, Kozerke S (2022) Preliminary experience of cardiac proton spectroscopy at 0.75 T. *NMR Biomed* 36:e4892
 43. Ahad J, Cummings E, Franson D, Hamilton J, Seiberlich N (2022) Optimization of through-time radial GRAPPA with coil compression and weight sharing. *Magn Reson Med* 88(3):1244–1254
 44. Lingala SG, Zhu Y, Lim Y, Toutios A, Ji Y, Lo WC et al (2017) Feasibility of through-time spiral generalized autocalibrating partial parallel acquisition for low latency accelerated real-time MRI of speech. *Magn Reson Med* 78(6):2275–2282
 45. Jaubert O, Montalt-Tordera J, Knight D, Coghlan GJ, Arridge S, Steeden JA et al (2021) Real-time deep artifact suppression using recurrent U-Nets for low-latency cardiac MRI. *Magn Reson Med* 86(4):1904–1916
 46. Nayak KS (2019) Response to letter to the editor: "Nomenclature for real-time magnetic resonance imaging." *Magn Reson Med* 82(2):525–526
 47. Fyrdahl A, Seiberlich N (2022) Real-time cardiac MRI at 0.55T using through-time spiral GRAPPA. In: ISMRM 2022; London, UK, p 1843
 48. Hamilton JI, Truesdell W, Galizia M, Burris N, Agarwal P, Seiberlich N (2023) A low-rank deep image prior reconstruction for free-breathing ungated spiral functional CMR at 0.55 T and 1.5 T. *MAGMA* 36:451–464
 49. Wang Z, Feng X, Mugler J, Salerno M, Campbell-Washburn A, Meyer C (2021) Spiral-in-out bSSFP real-time cine on a high performance 0.55T scanner. In: ISMRM 2021; Virtual, p 504
 50. Yagiz E, Garg P, Nayak KS, Tian Y (2023) Simultaneous multi-slice (SMS) real-time cardiac MRI at 0.55T. In: SCMR 2023; San Diego, US, p 1357579

51. Schuster A, Hor KN, Kowallick JT, Beerbaum P, Kutty S (2016) Cardiovascular magnetic resonance myocardial feature tracking: concepts and clinical applications. *Circ Cardiovasc Imaging* 9(4):e004077
52. Ibrahim E-S (2011) Myocardial tagging by cardiovascular magnetic resonance: evolution of techniques—pulse sequences, analysis algorithms, and applications. *J Cardiovasc Magn Reson* 13(1):36
53. Tian Y, Cui SX, Garg P, Nayak KS (eds) (2023) Opportunities for improved myocardial first-pass perfusion imaging at 0.55T. In: *ISMRM 2023*; Toronto, Canada. p 4283
54. Bandettini WP, Christine M, Shanbhag SM, Henry JL, Lowery MM, Chen MY et al (eds) (2021) A Comparison of Metal Artifacts in Cardiovascular MRI at 0.55T and 1.5T. In: *ISMRM annual meeting 2021*. p 3636
55. Li B, Lee NG, Cui SX, Nayak KS (2022) Lung parenchyma transverse relaxation rates at 0.55 Tesla. *Magn Reson Med* 89:1522–1530
56. Yu J, Xue Y, Song HK (2011) Comparison of lung T2* during free-breathing at 1.5 T and 3.0 T with ultrashort echo time imaging. *Magn Reson Med* 66(1):248–254
57. Campbell-Washburn AE, Malayeri AA, Jones EC, Moss J, Fennelly KP, Olivier KN et al (2021) T2-weighted lung imaging using a 0.55-T MRI system. *Radiol Cardiothorac Imaging*. 3(3):e200611
58. Wieslander Br, Javed A, Ramasawmy R, Malayeri AA, Baute S, O'Brien KJ, et al., editors. Lung nodule imaging using high-performance 0.55T MRI. *ISMRM 2022 Workshop on Low Field MRI*; 2022; virtual.
59. Azour L, Condos R, Keerthivasan MB, Bruno M, Pandit Sood T, Landini N et al (2022) Low-field 0.55 T MRI for assessment of pulmonary groundglass and fibrosis-like opacities: Inter-reader and inter-modality concordance. *Eur J Radiol* 156:110515
60. Campbell-Washburn AE, Suffredini AF, Chen MY (2021) High-performance 0.55-t lung MRI in patient with COVID-19 infection. *Radiology* 299(2):E246–E247
61. Heiss R, Grodzki DM, Horger W, Uder M, Nagel AM, Bickelhaupt S (2021) High-performance low field MRI enables visualization of persistent pulmonary damage after COVID-19. *Magn Reson Imaging* 76:49–51
62. Hinsen M, Nagel AM, May MS, Wiesmueller M, Uder M, Heiss R (2023) Lung nodule detection with modern low-field MRI (0.55 T) in comparison to CT. *Invest Radiol*. <https://doi.org/10.1097/RLI.0000000000001006>
63. Bhattacharya I, Ramasawmy R, Javed A, Chen MY, Benkert T, Majeed W et al (2021) Oxygen-enhanced functional lung imaging using a contemporary 0.55 T MRI system. *NMR Biomed* 34(8):e4562
64. Bhattacharya I, Ramasawmy R, Javed A, Lowery M, Henry J, Mancini C et al (2022) Assessment of lung structure and regional function using 0.55 T MRI in patients with lymphangioliomatosis. *Invest Radiol* 57(3):178–186
65. Javed A, Ramasawmy R, O'Brien K, Mancini C, Su P, Majeed W et al (2022) Self-gated 3D stack-of-spirals UTE pulmonary imaging at 0.55T. *Magn Reson Med* 87(4):1784–1798
66. Seemann F, Javed A, Chae R, Ramasawmy R, O'Brien K, Baute S et al (2022) Imaging gravity-induced lung water redistribution with automated inline processing at 0.55 T cardiovascular magnetic resonance. *J Cardiovasc Magn Reson* 24(1):35
67. Bieri O, Pusterla O, Bauman G (2022) Free-breathing half-radial dual-echo balanced steady-state free precession thoracic imaging with wobbling Archimedean spiral pole trajectories. *Z Med Phys* 33:220–229
68. Bauman G, Bieri O (2020) Balanced steady-state free precession thoracic imaging with half-radial dual-echo readout on smoothly interleaved archimedean spirals. *Magn Reson Med* 84(1):237–246
69. Bauman G, Lee NG, Tian Y, Bieri O, Nayak KS (2023) Submillimeter lung MRI at 0.55 T using balanced steady-state free precession with half-radial dual-echo readout (bSTAR). *Magn Reson Med* 90:1949–1957
70. Komlosi P, Altes TA, Qing K, Mooney KE, Miller GW, Mata JF et al (2017) Signal-to-noise ratio, T2, and T2* for hyperpolarized helium-3 MRI of the human lung at three magnetic field strengths. *Magn Reson Med* 78(4):1458–1463
71. Salerno M, Brookeman JR, de Lange EE, Mugler JP (2005) Hyperpolarized 3He lung imaging at 0.5 and 1.5 Tesla: a study of susceptibility-induced effects. *Magn Reson Med* 53(1):212–216
72. Merkle EM (2023) The potential of low-field MRI in abdominal imaging. *Eur Radiol* 33:6981–6983
73. Ge Y, Steel K, Antiochos P, Bingham S, Abdullah S, Mikolich JR et al (2021) Stress CMR in patients with obesity: insights from the Stress CMR perfusion imaging in the United States (SPINS) registry. *Eur Heart J Cardiovasc Imaging* 22(5):518–527
74. de Jonge CS, Smout AJPM, Nederveen AJ, Stoker J (2018) Evaluation of gastrointestinal motility with MRI: a dvances, challenges and opportunities. *Neurogastroenterol Motil* 30(1):e13257
75. Chandarana H, Bagga B, Huang C, Dane B, Petrocelli R, Bruno M et al (2021) Diagnostic abdominal MR imaging on a prototype low-field 0.55 T scanner operating at two different gradient strengths. *Abdom Radiol (NY)*. 46(12):5772–5780
76. Ramachandran A, Hussain H, Lala M, Richardson J, Dudek N, Morehouse J et al (eds) (2023) Abdominal MRI at 0.55 T: initial evaluation and optimization in healthy subjects. In: *ISMRM annual meeting 2023*; Toronto, Canada. p 1763
77. Liu Y, Hamilton J, Jiang Y, Seiberlich N (2022) Assessment of MRF for simultaneous T1 and T2 quantification and water-fat separation in the liver at 0.55 T. *MAGMA* 36:513–523
78. Guenther C, Koken P, Boernert P, Kozerke S (eds) (2021) Abdominal water/fat separated MR fingerprinting on a lower-field 0.75T MRI. In: *ISMRM 2021 annual meeting*; 2021; virtual. p 1557
79. Khodarahmi I, Keerthivasan MB, Brinkmann IM, Grodzki D, Fritz J (2023) Modern Low-field MRI of the musculoskeletal system: practice considerations, opportunities, and challenges. *Invest Radiol* 58(1):76–87
80. Meyer CH, Pauly JM, Macovski A, Nishimura DG (1990) Simultaneous spatial and spectral selective excitation. *Magn Reson Med* 15(2):287–304
81. Krinsky G, Rofsky NM, Weinreb JC (1996) Nonspecificity of short inversion time inversion recovery (STIR) as a technique of fat suppression: pitfalls in image interpretation. *AJR Am J Roentgenol* 166(3):523–526
82. Rutt BK, Lee DH (1996) The impact of field strength on image quality in MRI. *J Magn Reson Imaging* 6(1):57–62
83. Breit HC, Vosschenrich J, Hofmann V, Rusche T, Kovacs BK, Bach M et al (2023) Image quality of lumbar spine imaging at 0.55T low-field MRI is comparable to conventional 1.5T MRI—initial observations in healthy volunteers. *Acad Radiol* 30:2440–2446
84. Lopez Schmidt I, Haag N, Shahzadi I, Frohwein LJ, Schneider C, Niehoff JH et al (2023) Diagnostic image quality of a low-field (0.55T) knee MRI protocol using deep learning image reconstruction compared with a standard (1.5T) knee MRI protocol. *J Clin Med* 12(5):1916
85. Matsuura H, Inoue T, Konno H, Sasaki M, Ogasawara K, Ogawa A (2002) Quantification of susceptibility artifacts produced on high-field magnetic resonance images by various biomaterials used for neurosurgical implants. *Techn Note J Neurosurg* 97(6):1472–1475

86. Basar B, Sonmez M, Yildirim DK, Paul R, Herzka DA, Kocaturk O et al (2021) Susceptibility artifacts from metallic markers and cardiac catheterization devices on a high-performance 0.55 T MRI system. *Magn Reson Imaging* 77:14–20
87. Peeters JM, van Faassen EE, Bakker CJ (2006) Magnetic resonance imaging of microstructure transition in stainless steel. *Magn Reson Imaging* 24(5):663–672
88. Schenck JF (1996) The role of magnetic susceptibility in magnetic resonance imaging: MRI magnetic compatibility of the first and second kinds. *Med Phys* 23(6):815–850
89. Khodarahmi I, Brinkmann IM, Lin DJ, Bruno M, Johnson PM, Knoll F et al (2022) New-generation low-field magnetic resonance imaging of hip arthroplasty implants using slice encoding for metal artifact correction: first in vitro experience at 0.55 T and comparison With 1.5 T. *Invest Radiol* 57(8):517–526
90. Keskin K, Hargreaves BA, Nayak KS (eds) (2022) Imaging near metal at 0.55 T using gradient-echo based sequences: feasibility and opportunities. In: ISMRM 2022. p 957
91. Lim Y, Kumar P, Nayak KS (2023) Speech production RT-MRI at 0.55 Tesla. *Magn Reson Med*. <https://doi.org/10.1002/mrm.29843>
92. Chaudhari AJL, Cui Y, Bayne SX, Szabo CO, Boutin RM, Nayak RD, Krishna S (2023) Real-time MRI of the moving wrist at 0.55 Tesla. *Br J Radiol*. 96(1151):20230298. <https://doi.org/10.1259/bjr.20230298>
93. Splendiani A, Perri M, Grattacaso G, Di Tunno V, Marsecano C, Panebianco L et al (2016) Magnetic resonance imaging (MRI) of the lumbar spine with dedicated G-scan machine in the upright position: a retrospective study and our experience in 10 years with 4305 patients. *Radiol Med* 121(1):38–44
94. Nordberg CL, Boesen M, Fournier GL, Bliddal H, Hansen P, Hansen BB (2021) Positional changes in lumbar disc herniation during standing or lumbar extension: a cross-sectional weight-bearing MRI study. *Eur Radiol* 31(2):804–812
95. Aarvold A, Lohre R, Chhina H, Mulpuri K, Cooper A (2020) Dynamic deformation of the femoral head occurs on weightbearing in Legg–Calves–Perthes disease: a translational pilot study. *Bone Jt Open* 1(7):364–369
96. Pai SA, Zhang H, Street J, Wilson DR, Brown SHM, Oxland TR (2021) Preliminary investigation of spinal level and postural effects on thoracic muscle morphology with upright open MRI. *JOR Spine* 4(1):e1139
97. Charest-Morin R, Zhang H, Shewchuk JR, Wilson DR, Phillips AE, Bond M et al (2021) Dynamic morphometric changes in degenerative lumbar spondylolisthesis: a pilot study of upright magnetic resonance imaging. *J Clin Neurosci* 91:152–158
98. Masciocchi C, Barile A, Satragno L (2000) Musculoskeletal MRI: dedicated systems. *Eur Radiol* 10(2):250–255
99. Ghazinoor S, Crues JV, Crowley C (2007) Low-field musculoskeletal MRI. *J Magn Reson Imaging* 25(2):234–244
100. Zlatkin MB, Hoffman C, Shellock FG (2004) Assessment of the rotator cuff and glenoid labrum using an extremity MR system: MR results compared to surgical findings from a multi-center study. *J Magn Reson Imaging* 19(5):623–631
101. Shellock FG, Bert JM, Fritts HM, Gundry CR, Easton R, Crues JV (2001) Evaluation of the rotator cuff and glenoid labrum using a 0.2-Tesla extremity magnetic resonance (MR) system: MR results compared to surgical findings. *J Magn Reson Imaging* 14(6):763–770
102. Raby N (2001) Magnetic resonance imaging of suspected scaphoid fractures using a low field dedicated extremity MR system. *Clin Radiol* 56(4):316–320
103. Savnik A, Malmskov H, Thomsen HS, Bretlau T, Graff LB, Nielsen H et al (2001) MRI of the arthritic small joints: comparison of extremity MRI (0.2 T) vs high-field MRI (1.5 T). *Eur Radiol* 11(6):1030–1038
104. Ejbjerg BJ, Narvestad E, Jacobsen S, Thomsen HS, Østergaard M (2005) Optimised, low cost, low field dedicated extremity MRI is highly specific and sensitive for synovitis and bone erosions in rheumatoid arthritis wrist and finger joints: comparison with conventional high field MRI and radiography. *Ann Rheum Dis* 64(9):1280–1287
105. Dixon WT (1984) Simple proton spectroscopic imaging. *Radiology* 153(1):189–194
106. Nayak KS, Cui SX, Tasdelen B, Yagiz E, Weston S, Zhong X et al (2023) Body composition profiling at 0.55T: feasibility and precision. *Magn Reson Med* 90:1114–1120
107. Guenther C, Dillinger H, Boernert P, Kozerke S (eds) (2021) Three-point dixon abdominal water/fat separation using a lower-field 0.75T MRI. In: ISMRM 2011 annual meeting; virtual. p 3844
108. Nayak K, Tasdelen B, Yagiz E, Cui S (2022) Ultra-fast water/fat imaging of the abdomen at 0.55T. In: ISMRM 2022; London, p 1809
109. Shih S-F, Cui S, Zhong X, Tasdelen B, Yagiz E, Nayak K et al (2022) Free-breathing liver fat quantification using radial acquisition on a high-performance 0.55T MRI system. In: ISMRM 2022; London, p 1807
110. Tian Y, Krishna SN (2023) Real-time water/fat imaging at 0.55T with spiral out-in-out-in sampling. *Magn Reson Med*. 1-11. <https://doi.org/10.1002/mrm.29885>
111. Zi R, Chandarana H, Block K (2022) Fat-separated radial 3D bSSFP imaging at low field using frequency-sweep RF saturation and XD-GRASP reconstruction. In: ISMRM 2022; London, p 318
112. Lee NG, Ramasawmy R, Lim Y, Campbell-Washburn AE, Nayak KS (2022) MaxGIRF: Image reconstruction incorporating concomitant field and gradient impulse response function effects. *Magn Reson Med* 88:691–710
113. Lee N, Keskin K, Zhao Z, Nayak K (2022) Higher-order image reconstruction with integrated gradient nonlinearity correction using a low-rank encoding operator. In: ISMRM 2022; London, p 5050
114. Wang Z, Ramasawmy R, Feng X, Campbell-Washburn AE, Mugler JP, Meyer CH (2023) Concomitant magnetic-field compensation for 2D spiral-ring turbo spin-echo imaging at 0.55T and 1.5T. *Magn Reson Med* 90:552–568
115. Ramasawmy R, Mugler JP, Javed A, Wang Z, Herzka DA, Meyer CH et al (2023) Concomitant field compensation of spiral turbo spin-echo at 0.55 T. *MAGMA* 36(3):465–475
116. Vahle T, Bacher M, Rigie D, Fenchel M, Speier P, Bollenbeck J et al (2020) Respiratory motion detection and correction for MR using the pilot tone: applications for MR and simultaneous PET/MR examinations. *Invest Radiol* 55(3):153–159
117. Anand S, Lustig M (2023) Beat pilot tone: versatile, contact-free motion sensing in MRI with radio frequency intermodulation. [arXiv:2306.10236](https://arxiv.org/abs/2306.10236)
118. Solomon E, Rigie DS, Vahle T, Paška J, Bollenbeck J, Sodickson DK et al (2021) Free-breathing radial imaging using a pilot-tone radiofrequency transmitter for detection of respiratory motion. *Magn Reson Med* 85(5):2672–2685
119. Muñoz F, Lim Y, Cui SX, Stark H, Nayak KS (2022) Evaluation of a novel 8-channel RX coil for speech production MRI at 0.55 T. *MAGMA* 36:419–426
120. Wang B, Siddiq SS, Walczyk J, Bruno M, Khodarahmi I, Brinkmann IM et al (2022) A flexible MRI coil based on a cable conductor and applied to knee imaging. *Sci Rep* 12(1):15010
121. Gassenmaier S, Küstner T, Nickel D, Herrmann J, Hoffmann R, Almansour H et al (2021) Deep learning applications in magnetic resonance imaging: has the future become present? *Diagnostics (Basel)* 11(12):2181

122. Lundervold AS, Lundervold A (2019) An overview of deep learning in medical imaging focusing on MRI. *Z Med Phys* 29(2):102–127
123. Knoll F, Hammernik K, Kobler E, Pock T, Recht MP, Sodickson DK (2019) Assessment of the generalization of learned image reconstruction and the potential for transfer learning. *Magn Reson Med* 81(1):116–128
124. Hammernik K, Klatzer T, Kobler E, Recht MP, Sodickson DK, Pock T et al (2018) Learning a variational network for reconstruction of accelerated MRI data. *Magn Reson Med* 79(6):3055–3071
125. Hyun CM, Kim HP, Lee SM, Lee S, Seo JK (2018) Deep learning for undersampled MRI reconstruction. *Phys Med Biol* 63(13):135007
126. Peng W, Feng L, Zhao G, Liu F (2022) Learning optimal K-space acquisition and reconstruction using physics-informed neural networks. In: 2022 IEEE/CVF conference on computer vision and pattern recognition (CVPR). IEEE Computer Society, pp 20762–20771
127. Radhakrishna CG, Ciuciu P (2023) Jointly learning non-Cartesian k-space trajectories and reconstruction networks for 2D and 3D MR imaging through projection. *Bioengineering* 10(2):158
128. Wang G, Nielsen JF, Fessler JA, Noll DC (2023) Stochastic optimization of three-dimensional non-Cartesian sampling trajectory. *Magn Reson Med* 90(2):417–431
129. Blansit K, Retson T, Masutani E, Bahrami N, Hsiao A (2019) Deep learning-based prescription of cardiac MRI planes. *Radiol Artif Intell* 1(6):e180069
130. Edalati M, Zheng Y, Watkins MP, Chen J, Liu L, Zhang S et al (2022) Implementation and prospective clinical validation of AI-based planning and shimming techniques in cardiac MRI. *Med Phys* 49(1):129–143
131. Chen C, Qin C, Qiu H, Tarroni G, Duan J, Bai W et al (2020) Deep learning for cardiac image segmentation: a review. *Front Cardiovasc Med* 7:25
132. Bien N, Rajpurkar P, Ball RL, Irvin J, Park A, Jones E et al (2018) Deep-learning-assisted diagnosis for knee magnetic resonance imaging: development and retrospective validation of MRNet. *PLoS Med* 15(11):e1002699
133. Chen Y, Ruan D, Xiao J, Wang L, Sun B, Saouaf R et al (2020) Fully automated multiorgan segmentation in abdominal magnetic resonance imaging with deep neural networks. *Med Phys* 47(10):4971–4982
134. Ayde R, Senft T, Salameh N, Sarracanie M (2022) Deep learning for fast low-field MRI acquisitions. *Sci Rep* 12(1):11394
135. Koonjoo N, Zhu B, Bagnall GC, Bhutto D, Rosen MS (2021) Boosting the signal-to-noise of low-field MRI with deep learning image reconstruction. *Sci Rep* 11(1):8248
136. Lau V, Xiao L, Zhao Y, Su S, Ding Y, Man C et al (2023) Pushing the limits of low-cost ultra-low-field MRI by dual-acquisition deep learning 3D superresolution. *Magn Reson Med* 90(2):400–416
137. Quick HH, Ladd ME, Hoevel M, Bosk S, Debatin JF, Laub G et al (2002) Real-time MRI of joint movement with trueFISP. *J Magn Reson Imaging* 15(6):710–715
138. Menys A, Taylor SA, Emmanuel A, Ahmed A, Plumb AA, Odille F et al (2013) Global small bowel motility: assessment with dynamic MR imaging. *Radiology* 269(2):443–450
139. Zhang S, Olthoff A, Frahm J (2012) Real-time magnetic resonance imaging of normal swallowing. *J Magn Reson Imaging* 35(6):1372–1379
140. Wu Z, Chen W, Khoo MC, Davidson Ward SL, Nayak KS (2016) Evaluation of upper airway collapsibility using real-time MRI. *J Magn Reson Imaging* 44(1):158–167
141. Martin MN, Jordanova KV, Kos AB, Russek SE, Keenan KE, Stupic KF (2023) Relaxation measurements of an MRI system phantom at low magnetic field strengths. *MAGMA* 36(3):477–485
142. Keenan KE, Gimbutas Z, Dienstfrey A, Stupic KF, Boss MA, Russek SE et al (2021) Multi-site, multi-platform comparison of MRI T1 measurement using the system phantom. *PLoS ONE* 16(6):e0252966
143. Sarracanie M, Salameh N (2020) Low-field MRI: how low can we go? A fresh view on an old debate. *Front Phys* 8:172

Publisher's Note Springer Nature remains neutral with regard to jurisdictional claims in published maps and institutional affiliations.